Nuclear Materials and Energy 41 (2024) 101779

Contents lists available at ScienceDirect

Nuclear Materials and Energy

journal homepage: www.elsevier.com/locate/nme

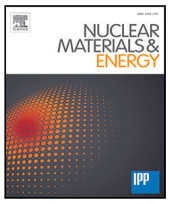

Experimental investigation of steady state power balance in double null and single null H mode plasmas in MAST Upgrade

J. Lovell [a,*], S.S. Henderson [b], J.M. Stobbs [b], A. Kirk [b], F. Federici [a], B.S. Patel [b], P.J. Ryan [b], J.R. Harrison [b], B.A. Lomanowski [a], J.D. Lore [a], The MAST Upgrade Team [1]

[a] Oak Ridge National Laboratory, Oak Ridge, TN, 37831, USA
[b] United Kingdom Atomic Energy Authority, Culham Campus, Abingdon, OX14 3DB, Oxon, UK

ARTICLE INFO

Keywords:
Power balance
Power exhaust
Tokamak
Alternative divertors

ABSTRACT

Global power balance calculations in steady state H mode plasmas varying the distance between separatrices (dr_{sep}) and the divertor configuration have been performed in MAST Upgrade. As dr_{sep} becomes more negative, more of the power crossing the separatrix goes to the lower divertor. The inner divertor receives a higher fraction of the power exhaust in a Super-X divertor plasma compared to a conventional divertor plasma at similar negative dr_{sep}, which is a concern for high power devices employing alternative divertor configurations for power exhaust handling. Global power accounting suggests > 30 % of the input power is unaccounted for with the power loss channels quantified in this work. Charge exchange and orbit losses from the NBI could account for a large fraction of unaccounted power but it is not possible to precisely determine this without further diagnostic calibration.

1. Introduction

Understanding power balance is important for the characterization and interpretation of divertor performance and detachment behaviour. The design and engineering of plasma-facing components (PFCs) and the choice of plasma operating scenario are strongly influenced by the distribution of power exhaust among all available power sinks.

Previous work has examined the impact on power sharing of double null vs. single null in conventional [1] and spherical [2,3] tokamak plasmas, as well as in advanced divertors [4], but the combined impact of advanced divertors, low aspect ratio and double null vs. single null in reactor-relevant H mode has not previously been quantified.

In this work we present new measurements of the power balance in H mode plasmas in MAST Upgrade, for both double null and single null plasma configurations with conventional and Super-X divertors. Section 2 describes the experiment setup, the power channels considered and the diagnostics and interpretive codes used to quantify each power channel. Section 3 examines the impact of the divertor configuration on the relative magnitude of each power loss channel. Section 4 assesses the total power accounting.

2. Experiment description

MAST Upgrade is a medium sized spherical tokamak built in part to study power exhaust solutions for future high power devices [5]. It typically operates in a connected double null configuration with either a conventional — short leg, low total flux expansion — divertor (CD) or a Super-X — long leg, high total flux expansion — divertor (SXD) configuration on the low field side (LFS) and a conventional high field side (HFS) divertor. All plasma-facing surfaces are graphite. Auxiliary heating is provided by 2 co-current tangential neutral beam injectors (NBI), one injecting at the midplane and one injecting 0.65 m above the midplane. The machine is nominally up/down symmetric.

In this work we have considered the global power balance in CD and SXD H mode plasmas with $I_p = 0.75$ MA, $B_t = 0.55$ T on axis, $\overline{n_e} = 3.5 \times 10^{19}$ m^{-3} to 6.5×10^{19} m^{-3} and auxiliary heating $P_{NBI} \leq 3.5$ MW. We focus on H mode plasmas with the maximum available heating power because of their greater reactor relevance, increased signal levels on the relevant power exhaust diagnostics and a reduction in the scrape off layer (SOL) heat flux width λ_q. The outboard λ_q was approximately 7 mm, measured using thermography [6]. Due to the up/down symmetry of the PF coils, we varied the distance between separatrices at the outboard midplane, dr_{sep}, by adjusting the vertical position of the plasma. We studied both connected double null (DN) plasmas with magnetic axis vertical position $Z_{mag} \approx 0$, giving $dr_{sep} = 0(2)$ mm, and also downshifted plasmas with $Z_{mag} \approx -10$ cm and $dr_{sep} = -10(2)$ mm, which we will term lower single null (LSN). 3 of the 4 plasmas studied were ELM-free in the time windows analysed, and

* Corresponding author.
E-mail address: lovelljj@ornl.gov (J. Lovell).
[1] See the author list of J. Harrison et al 2019 Nucl. Fusion 59 112011.

https://doi.org/10.1016/j.nme.2024.101779
Received 5 July 2024; Received in revised form 30 September 2024; Accepted 16 October 2024
Available online 23 October 2024

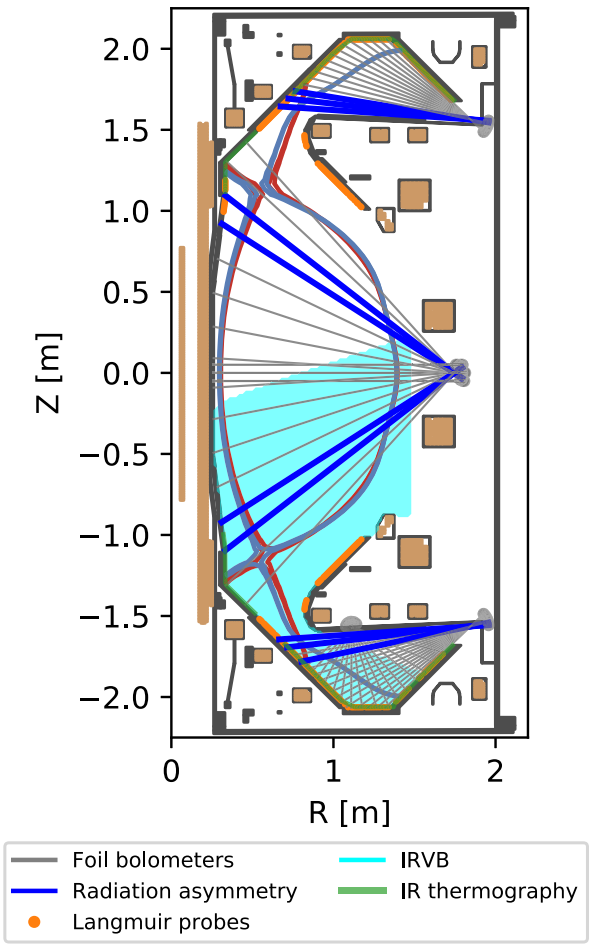

Fig. 1. Diagnostics used for power balance measurements. Grey lines show foil bolometer lines of sight, with the foil bolometers used for up/down radiation asymmetry estimates in blue. The cyan region is the field of view of the IRVB. Orange dots show target Langmuir probe positions and the green line is the poloidal projection of the analysis path used for IR thermography. Separatrices from representative DN CD (red) and SXD (blue) equilibria are also shown; the primary separatrices of the LSN CD and SXD cases (not shown) are similar to their respective DN cases. (For interpretation of the references to colour in this figure legend, the reader is referred to the web version of this article.)

whilst the DN CD plasma did have some ELMs these were generally not resolvable by the diagnostics used in the study. Our results therefore should be considered applicable to the inter-ELM phase in H mode.

2.1. Contributors to power balance

There are many contributors to the overall power balance. We present here what we consider to be the most significant contributors and which we are able to estimate with the available diagnostic set, illustrated in Fig. 1.

Power balance is satisfied when:

$$P_{NBI} + P_{Ohm} - \mathrm{d}W_p/\mathrm{d}t - P_{rad,c} = P_{rad,s} + P_{tgt} \quad (1)$$

On the left hand side of Eq. (1) are the terms which describe the power crossing the separatrix, P_{sep}. On the right are the terms which describe where and how P_{sep} is dissipated in the SOL and divertors: the total of these terms we will refer to as P_{div}. We will discuss potential missing terms in this equation later in Section 4.

P_{NBI} is the amount of NBI heating power coupled to the plasma, taken to be the injected power minus the shine-through as calculated using the TRANSP code [7] — we neglect charge exchange (CX) and orbit losses and neutral interactions between the injection location and the plasma here. P_{Ohm} is the Ohmic heating power and $\mathrm{d}W_p/\mathrm{d}t$ is the rate of change of plasma stored energy: both are calculated using EFIT [8].

$P_{rad,c}$ is the radiated power in the core plasma, estimated by a weighted sum of line-integral brightnesses from foil bolometers [9]. $P_{rad,s} = P_{rad,s,L} + P_{rad,s,U}$ is the radiation in the SOL region. $P_{rad,s,L}$, the radiation in the lower divertors, is estimated by integrating the emission from the inner leg, X point and outer leg regions using poloidal emissivity profiles from tomographic reconstructions of infra-red video bolometer (IRVB) measurements [10].

The upper divertor radiation $P_{rad,s,U}$ is estimated from the lower divertor radiation measured with the IRVB and a radiation asymmetry factor calculated from measurements of selected foil bolometer channels near the X point and in the divertors which had acceptable SNR. Taking the average brightness measurements B of these channels as $U = \langle B_{upper} \rangle$ and $L = \langle B_{lower} \rangle$ to obtain the up/down radiation asymmetry, we compute the upper divertor radiation as $P_{rad,s,U} = P_{rad,s,L} \times U/L$.

P_{tgt} is the power carried to the divertor target plates, defined as the integral of the perpendicular heat flux $q_\perp$ assuming toroidal symmetry:

$$P_{tgt} = \int_{tgt} 2\pi R q_\perp(s) \mathrm{d}s \quad (2)$$

Here R is the major radius, $\mathbf{s}$ is a vector parallel to the divertor surface in the poloidal direction (with magnitude s) and the integral is performed over the subset of the targets which are receiving power from the divertor legs.

$q_\perp(s)$ may be determined either from fitted current vs. voltage (IV) curves measured by divertor Langmuir probes [11] (LPs), which have extensive coverage of the outer divertors, or from thermography using a suite of infra red (IR) cameras which cover all 4 divertors [12]. This calculation required particular care due to a number of confounding factors in the raw data: a detailed description of these factors and how we dealt with them is presented in Section 2.2.

2.2. Estimating the power on the divertor targets

There are several sources of error to be aware of when estimating the total power to the divertor targets using LPs and IR thermography. First, the routine LP analysis performed on MAST-U typically overestimates the electron temperature T_e for low T_e ($\ll$10 eV) which in turn results in $q_\perp$ being overestimated: this is typical for LPs [11]. To avoid this the use of LPs for heat flux analysis should therefore be restricted to attached divertor conditions: generally this means high power low density plasmas and only the lower divertors in LSN cases.

Second, in this work we have assumed toroidal symmetry in both the LP and IR analysis when calculating the total power from the poloidal heat flux profile. However, we know of several potential sources of toroidally-asymmetric heat fluxes, including partial wetting of the divertor tiles (both intentionally to avoid leading edges and unintentionally due to installation tolerances) and toroidal field ripple (due to discrete TF coils, an intrinsic $n = 2$ error field and an $n = 24$ error field local to the HFS strike point). We mitigated the impact of toroidal asymmetries by placing the strike points away from regions of strong toroidal asymmetry: this was mostly successful except at the inner divertor in the LSN SXD configuration where we instead calculated the heat flux along 10 poloidal paths with different toroidal angles and averaged them to produce a toroidally-averaged poloidal heat flux profile.

Fig. 2 illustrates two additional potential sources of error from IR thermography. A surface layer (possibly redeposited sputtered graphite) around $R = 1.35$ m with very different thermal properties to the bulk divertor tile leads to an over-estimate of the heat flux in steady state but is easily detectable due to its apparent negative heat flux immediately after transients. This region is excluded from the integral in Eq. (2),

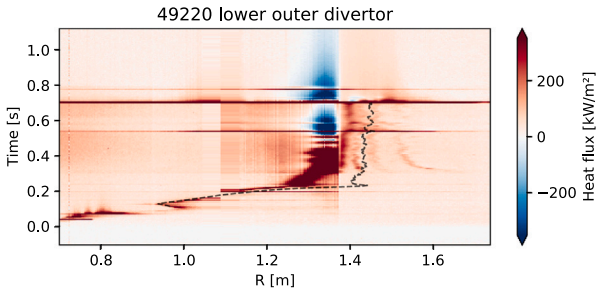

Fig. 2. Calculated target heat flux at the LFS strike point in a SXD plasma, with the EFIT-estimated strike point position (dashed line). After the transient event at 0.55 s and the end of the flat top at 0.7 s the heat flux around $R = 1.35$ m appears to become negative.

though we must ensure the strike point is far enough outside this region to avoid missing significant power. A broad apparent background heat flux over the entire field of view of the IR camera, due to both intrinsic plasma IR emission [12] and tile reflectivity can lead to an overestimation of the total power. We avoid this by further restricting the integral in Eq. (2) to a narrow region around the strike point just wide enough to encompass the SOL heat flux: a range of between ±10 cm and ±20 cm (chosen by hand for each divertor in each pulse) from the EFIT-computed strike point position was sufficient.

2.3. Data validation

Power balance studies require accurate and precise diagnostic measurements, with well-quantified uncertainties. In practice this is an extremely difficult task to perform for each diagnostic individually. We instead employ multiple diagnostics providing independent measurements of some of the quantities in Eq. (1) to perform diagnostic cross-comparisons for a basic uncertainty quantification.

Fig. 1 shows that the foil bolometers and IRVB have an overlapping view of the lower half of the plasma core. When the assumption of up/down radiation symmetry holds, the total core radiated power calculated with the foil bolometers should be double the total radiated power calculated by integrating the part of the emissivity profile reconstructed from IRVB measurements within the last closed flux surface. Fig. 3 (top) shows such a comparison for the DN CD shot used in this study. During the I_p flat top phase the two diagnostics agree to within 20%, with a maximal discrepancy of approximately 200 kW.

Given the confounding factors presented in Section 2.2 it is important to verify that the total power calculated from IR thermography is a reliable estimate, particularly as it is the only method available for the HFS divertors. Fig. 3 (bottom) shows the total power to the lower outer divertor leg calculated from IR and LP analysis for a DN CD shot with attached divertors. As with the radiated power, there is good agreement between the two independent measurements with <10% variation, suggesting a high level of accuracy and precision in the target power calculation in this scenario.

3. Distribution of power exhaust

Fig. 4 shows the relative distribution of P_{div}, with P_{tgt} resolved into all 4 divertors and $P_{rad,s}$ resolved into upper and lower SOL regions, for the 4 different plasma configurations studied in this work. Each plot shows the distribution averaged over a time window in which both the plasma conditions and power exhaust were approximately stationary, though some ELM averaging has been done in the DN CD case as the ~50 Hz ELM frequency was too high to obtain a single inter-ELM window of sufficient length. We also calculated the power measured by Langmuir probes on the passive stability plate armour — the diagonal

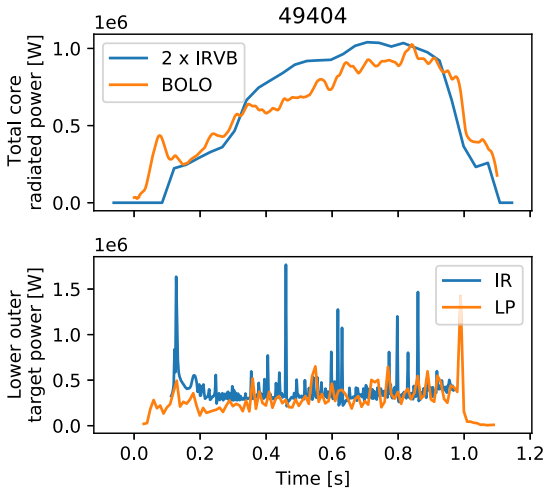

Fig. 3. Top: comparison of the total core radiated power calculated from foil bolometers and from the IRVB assuming up down symmetry. The two measurements agree to within 20 % during the I_p flat top phase between 100 ms and 950 ms. Bottom: comparison of total power carried to the lower outer divertor calculated using IR thermography and LP analysis, showing good agreement for the inter-ELM total power.

features outboard of the X points in Fig. 1 — but this was < 1% of the total P_{div} and so can be neglected.

The DN cases have well balanced divertor target heat loads in both divertor configurations, though there is a pronounced SOL radiation asymmetry in favour of the upper divertor. 15% to 20% of the target heat load goes to the inner divertor in both cases. The SOL radiated fraction is also similar in both cases despite the greater expected dissipation capability of the SXD: this could perhaps be explained by the ~25% higher upstream density in the CD plasma but a detailed discussion of the cause is beyond the scope of this manuscript.

It is immediately apparent that moving from DN to LSN causes a redistribution of the power from the upper divertors to the lower divertors; this is true in both CD and SXD cases. Both the power carried by the plasma to the targets and the up/down radiation asymmetry become more strongly biased towards the lower divertors. However, there is still an appreciable fraction of the power going to the upper divertors: an indication that these plasmas are not fully single null. This is consistent with previous work [1–4] where values of $|\mathrm{d}r_{sep}/\lambda_q|$ significantly larger than the ~1 we were able to achieve here were required to effectively suppress power loading to the secondary divertors.

The final important feature to note is that the LSN SXD has a significantly larger power fraction going to the lower inner target than all the other configurations, even the LSN CD case (both scenarios had similar inner gaps of 2.5 cm to 3 cm in the time window analysed). In fact the power load on the inner target is only about 30% less than that on the outer target. The increase in the relative inner target power loading is in qualitative agreement with what was predicted in previous work [4,13], based on a model of the poloidal heat flux q_p derived from the 2-point model in the conduction limited regime and considering the inverse-major-radius-weighted connection lengths $\mathcal{L}_\parallel$ of inner and outer divertor flux tubes [13]:

$$q^{in}_{p,u}/q^{out}_{p,u} = \mathcal{L}_{\parallel,out}/\mathcal{L}_{\parallel,in} \tag{3}$$

This model predicts the power asymmetry P_{inner}/P_{outer}, where $P = \int q_{p,u}\mathrm{d}r$ across the SOL, to be 0.21 for the CD LSN, in good agreement with the 0.22 measured (Fig. 4). However, in the SXD LSN case the model predicts $P_{inner}/P_{outer} = 0.33$, whereas we measure 0.70. This discrepancy can be at least partially explained by the enhanced SOL dissipation in the SXD case, shown by the increased SOL radiation, which is not accounted for in the model.

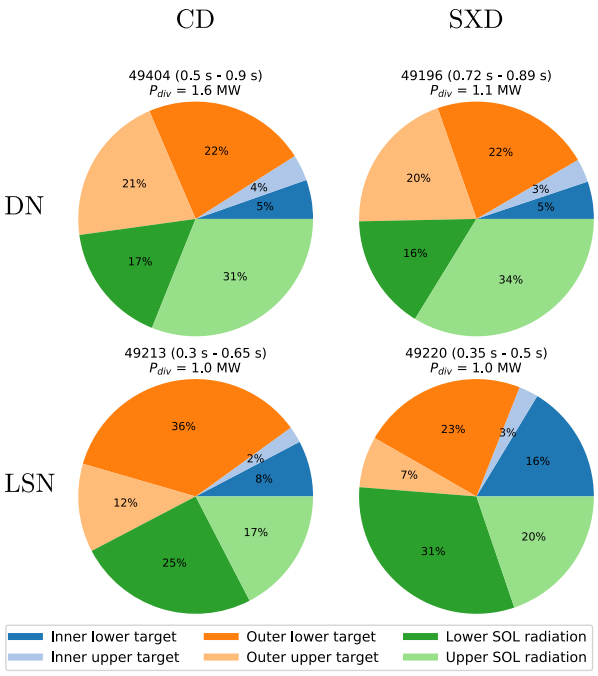

Fig. 4. Distribution of P_{div} among the loss channels considered: power conducted to each of the 4 divertor targets and the power radiated in the upper and lower SOL. CD plasmas are on the left, SXD on the right. DN plasmas are on the top row, LSN on the bottom.

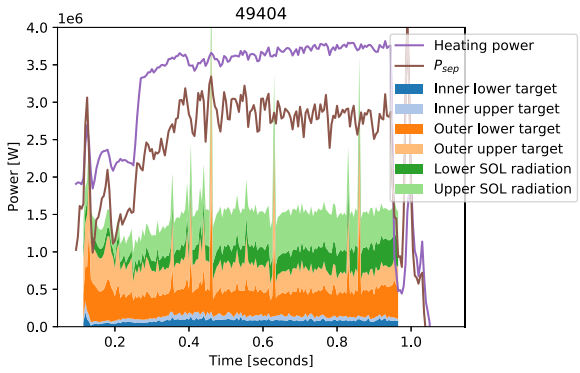

Fig. 5. Total power accounting for the DN CD case. The lines represent the input power and the power crossing the separatrix into the SOL, and the filled areas represent the cumulative power in each the power loss channels presented in Section 3.

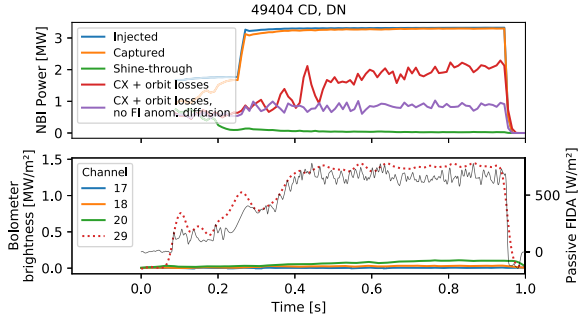

Fig. 6. Top: neutral beam heating and loss power. Bottom: brightness measurements from a foil bolometer (channel 29) sensitive to fast neutrals as well as plasma radiation compared with bolometers viewing a similar region of the plasma but not sensitive to fast neutrals, along with inter-ELM line-integral passive FIDA measurements at tangency radius 1.35 m. After 400 ms the CX + orbit losses predicted by TRANSP increase in time unless fast ion anomalous diffusion is neglected, whereas the bolometer signal and FIDA losses are both constant.

This increase in the relative power loading of the inner divertor gives cause for concern, as the inner target has a much lower wetted area than the outer target (especially in a long-legged SXD divertor) so the peak heat flux will be significantly larger. It appears operating close to double null is key for divertor configurations designed to ease power handling at the outer divertor to avoid making power handling at the inner divertor harder: further studies to determine the generality of this result and the physical mechanisms responsible are required to understand its implications for reactors.

4. Total power accounting

Finally, we present the results of total power accounting to investigate whether we can completely account for all of the input power in the measured loss channels defined in Eq. (1). The analysis has been performed for all 4 cases presented in Section 3 with essentially the same outcome for all 4: for brevity we present only the DN CD case here.

Fig. 5 shows the time-resolved power accounting throughout the DN CD discharge. After 400 ms the plasma is in an approximately stationary ELMy H mode with steady shape, stored energy and core density and temperature. The total heating power is around 3.7 MW, with P_{NBI} = 3.3 MW and P_{Ohm} = 0.4 MW. Slightly less than 1 MW of this is lost as core radiation (on average dW_p/dt is negligible in this phase), leaving a little under 3 MW crossing the separatrix. Of this, a total of 1.6 MW is distributed among the power loss channels we measure. This leaves just under 1.5 MW of power unaccounted for. Though not shown here, the other 3 cases studied all had between 1.5 MW and 1.8 MW of "missing" power — the power deficit here appears independent of divertor configuration and dr_{sep}. Although we are not properly capturing the ELM energy due to limited time resolution, the power deficit is the same in ELM-free phases of the other cases so this does not affect our conclusions.

It is important to note that a significant power deficit is not unique to this work. Detailed energy balance studies on JET found approximately 25% of the input power was unaccounted for [14], while detachment studies on TCV have found that between 1/4 and 2/3 of the power calculated to be crossing the separatrix was unaccounted for [4,15]. Energy deficits as low as 5% have been found on ASDEX Upgrade using whole-pulse cooling water calorimetry [16] but this method is unable to resolve individual phases of the pulse.

It is natural to ask where this missing power may be going. A loss channel which we have neglected is fast ion losses, in particular charge-exchange, orbit and anomalous losses. ASCOT modelling of early MAST-U discharges found fast particle charge exchange losses of around 20% of the input power [17] — this could explain ~0.6 MW of the missing power but precise quantitative predictions using this method are still pending outstanding diagnostic calibrations. TRANSP does estimate these losses but interpretive runs constrained to reproduce the pulse's measured neutron rate by adjusting the fast ion anomalous diffusion predict orbit losses which increase linearly in time in the latter part of the pulse. This is qualitatively inconsistent with both the steady state divertor power loading shown in Fig. 5 and measurements from foil bolometer channels sensitive to fast neutrals [9] and passive fast ion D-alpha (FIDA) measurements ~4 cm inside the separatrix, which both suggest no time evolution of the losses as shown in Fig. 6. Neglecting anomalous diffusion does give a qualitative match to the bolometry and FIDA and provides a lower bound on fast particle losses of ~0.9 MW but results in an over-estimation of the neutron rate. This inability to reconcile the neutron rate and the qualitative bolometry and power exhaust measurements shows that the fast neutral loss fraction is therefore not yet well constrained.

Toroidally asymmetric losses outside of areas with diagnostic coverage are also possible. Ionizing the fuelling gas sinks power near

the fuelling location and these pulses have only one fuelling location active, on the centre column slightly toroidally displaced from the foil bolometers and out of view of the IRVB. Most of this energy is likely to be radiated but may not be captured by the bolometers. Similarly, LP and IR diagnostics only cover subsets of the divertor targets and so strong toroidal asymmetries in the target power deposition may not be detectable (there is already evidence for some of these as described in Section 2.2). While we determined negligible power is being scraped off on the LFS passive stability plates, it is possible that some power is being scraped off on the centre column at the HFS due to the small inner gap to the separatrix, which varies between 2.5 cm in LSN to 4 cm in DN. There is no LP or routine IR coverage here and even non-routine IR measurements on the centre column, while possible to arrange, would struggle to distinguish IR emission due to heated tiles from intrinsic plasma IR emission. However, the insensitivity of the power deficit to plasma shape (including inner gap) does suggest that any power losses on the centre column are small compared with the total power deficit.

Finally, it is possible that some power is lost before it is even coupled to the plasma, in the NBI beam lines. Future work will estimate the extent of this contribution by varying the NBI heating power and observing the impact on the power deficit.

5. Conclusions and future work

We have found that in both DN and LSN H mode plasmas the majority of the power crossing the separatrix goes to the outer divertor legs, though we did not completely remove all power to the upper divertor in the LSN cases studied here. The inner divertor receives a significantly higher fraction of the power in LSN SXD compared with LSN CD, which is a concern for future high power devices which aim to use highly dissipative outer divertors for power handling and may place increased demands on either the inner target heat loading (or power dissipation) capability or tighter control of double null geometry. The extent to which this in/out asymmetry varies with the amount of dissipation in the outer divertor is an important unanswered question for which further study is required: solving the outer divertor exhaust problem may in fact be simply moving the trouble elsewhere.

We have also seen a significant power deficit whereby >30% of the input power is unaccounted for in the exhaust channels that we measure, though this may be reduced to ~15% by including an approximate estimate of fast particle losses. While this is slightly – but not dramatically – worse than the outcomes of time-resolved power balance measurements on other machines, it does pose the question of where this additional power is going. On a higher powered device like a reactor this amount of missing power could do serious damage if it were deposited on components not designed for high power loading. Further studies exploring the correlation of missing power with input and exhaust power channels are planned to aid in determining the source of this missing power.

CRediT authorship contribution statement

J. Lovell: Writing – review & editing, Writing – original draft, Visualization, Validation, Software, Methodology, Investigation, Formal analysis, Data curation, Conceptualization. **S.S. Henderson:** Resources, Project administration, Methodology, Investigation, Conceptualization. **J.M. Stobbs:** Writing – review & editing, Validation, Software, Formal analysis. **A. Kirk:** Writing – review & editing, Validation, Software, Investigation, Formal analysis, Data curation. **F. Federici:** Validation, Investigation, Formal analysis, Data curation. **B.S. Patel:** Writing – review & editing, Validation, Software, Investigation, Formal analysis. **P.J. Ryan:** Validation, Formal analysis, Data curation. **J.R. Harrison:** Writing – review & editing, Resources, Investigation, Conceptualization. **B.A. Lomanowski:** Supervision, Methodology, Conceptualization. **J.D. Lore:** Writing – review & editing, Supervision, Funding acquisition,.

Declaration of competing interest

The authors declare that they have no known competing financial interests or personal relationships that could have appeared to influence the work reported in this paper.

Acknowledgements

This work was supported by the US DOE under award DE-AC05-00OR22725 and by the EPSRC, UK Energy Programme grant EP/W006839/1. The authors would like to thank Clive Michael of UCLA for providing the passive FIDA data presented in Section 4.

Data availability

Data will be made available on request.

References

[1] D. Brunner, et al., Nucl. Fusion 58 (7) (2018) 076010.
[2] A. Kirk, et al., Plasma Phys. Control. Fusion 46 (3) (2004) 551.
[3] G.D. Temmerman, et al., Plasma Phys. Control. Fusion 52 (9) (2010) 095005.
[4] O. Février, et al., Nucl. Fusion 61 (11) (2021) 116064.
[5] W. Morris, et al., IEEE Trans. Plasm. Sci. 46 (5) (2018) 1217–1226.
[6] J.R. Harrison, et al., Plasma Phys. Control. Fusion 66 (6) (2024) 065019.
[7] J. Breslau, et al., TRANSP, Computer Software (2018) http://dx.doi.org/10.11578/dc.20180627.4.
[8] L.L. Lau, et al., Nucl. Fusion 25 (11) (1985) 1611.
[9] J. Lovell, et al., Rev. Sci. Instrum. 94 (2) (2023) 023509.
[10] F. Federici, et al., Rev. Sci. Instrum. 94 (3) (2023) 033502.
[11] P.J. Ryan, et al., Rev. Sci. Instrum. 94 (10) (2023) 103501.
[12] J.M. Stobbs, et al., Rev. Sci. Instrum. in review.
[13] R. Maurizio, et al., Nucl. Mater. Energy 19 (2019) 372–377.
[14] G.F. Matthews, et al., Nucl. Mater. Energy 12 (2017) 227–233.
[15] J.R. Harrison, et al., Plasma Phys. Control. Fusion 61 (6) (2019) 065024.
[16] A. Redl, et al., Plasma Phys. Control. Fusion 65 (11) (2023) 115003.
[17] P. Ollus, et al., Plasma Phys. Control. Fusion 66 (2) (2023) 025009.